The Spine Journal 19 (2019) 931–941

Basic Science

Optimal satellite rod constructs to mitigate rod failure following pedicle subtraction osteotomy (PSO): a finite element study

Ardalan Seyed Vosoughi, MS[a], Amin Joukar, MS[a], Ali Kiapour, PhD[a], Dikshya Parajuli, BS[a], Anand K. Agarwal, MD[a], Vijay K. Goel, PhD[a,*], Joseph Zavatsky, MD[b]

[a] *Engineering Center for Orthopaedic Research Excellence (ECORE), Departments of Bioengineering and Orthopaedics surgery, Colleges of Engineering and Medicine, University of Toledo, 5046 NI, MS 303, Toledo, OH 43606, USA*
[b] *Spine & Scoliosis Specialists, 10908 Ridgedale Road, Tampa, FL 33617, USA*
Received 20 June 2018; revised 1 November 2018; accepted 2 November 2018

Abstract

BACKGROUND CONTEXT: Pedicle subtraction osteotomy (PSO) is a challenging restoration technique for sagittal imbalance and is associated with significant complications. One of the major complications is rod fracture and there exists a need for a biomechanical assessment of this complication for various instrumentation configurations.

PURPOSE: To evaluate and compare the global range of motion (ROM), rod stress distribution, and the forces on the pedicle subtraction site in various instrumentation configurations using finite element analysis.

STUDY DESIGN/SETTING: A computational biomechanical analysis.

METHODS: A previously validated osseoligamentous three-dimensional spinopelvic finite element model (T10-pelvis) was used to develop a 30° PSO at the L3 level. In addition to the standard bilateral cobalt chromium primary rod instrumentation of the PSO model, various multirod configurations including constructs with medially, laterally, and posteriorly affixed satellite rods and the short-rod technique were assessed in spinal physiological motions. T10-S1 global ROM, maximum von Mises stress on the rods and at the PSO level, factor of safety (yield stress of the rod material/maximum actual stress in the rod) and the load acting across the PSO site were compared between various instrumentation configurations. The higher the factor of safety the lesser the chances of rod failure.

RESULTS: Among all multirod constructs, posteriorly affixed satellite rod construct showed the greatest motion reduction compared to the standard bilateral rod configuration followed by medially and laterally affixed satellite rod constructs. Compared to the standard bilateral rod configuration, recessed short-rod technique resulted in 4% to 49% reduction in T10-S1 ROM recorded in extension and lateral bending motions, respectively, while the axial rotation motion increased by approximately 31%. Considering the maximum stress values on the rods, the recessed short-rod technique showed the greatest factor of safety (FOS = 4.1) followed by posteriorly (FOS = 3.9), medially (FOS = 3), laterally affixed satellite rod constructs (FOS = 2.8), and finally the standard bilateral rod construct (FOS = 2.7). By adding satellite rods, the maximum von Mises stress at the PSO level of the rods also reduced significantly and at this level resulted in the greatest FOS in the posteriorly affixed satellite rod construct. Compared to the

FDA device/drug status: Not applicable.

Author disclosures: ***ASV:*** Grant: NSF (D, paid directly to institution). ***AJ:*** Grant: NSF (D, paid directly to institution). ***AK:*** Nothing to disclose. ***DP:*** Grant: NSF (D, paid directly to institution). ***AKA:*** Grant: NSF (D, paid directly to institution). Royalties: Joimax GmbH (B), Paradigm Spine GmbH (C). Stock Ownership: Osteonovus Inc (, 22%), Spinal Balance Inc (, 24%). ***VKG:*** Grant: NSF (D, paid directly to institution), NSF/CDMI (F, outside the submitted work, paid directly to institution). Royalties: University of Toledo (C). Stock Ownership: Spinal Balance, OsteoNovus. ***JZ:*** Grant: NSF (D, paid directly to institution), AO Spine (D, outside submitted work, paid directly to institution). Royalties: Zimmer Biomet (D). Stock Ownership: Vivex (<1%). Consulting: Depuy Synthes, Stryker, Zimmer Biomet (B).

* Corresponding author. Engineering Center for Orthopaedic Research Excellence (E-CORE), Departments of Bioengineering and Orthopaedic Surgery, Colleges of Engineering and Medicine, University of Toledo, 5046 NI, MS 303, Toledo, OH 43606, USA. Tel.: 419-530-8035; fax: 419-530-8076.

E-mail address: Vijay.Goel@utoledo.edu (V.K. Goel).

https://doi.org/10.1016/j.spinee.2018.11.003

standard bilateral rod construct, the load magnitude acting on the osteotomy site decreased by 11%, 16%, and 37% in the laterally, medially, and posteriorly affixed satellite rod constructs, respectively, and did not change with the short-rod technique.

CONCLUSIONS: Adding satellite rods increases the rigidity of the construct, which results in an increase in the stability and the reduction of the global ROM. Additionally, having satellite rods reduces the stress on the primary rods at the PSO level and shifts the stresses from this PSO region to areas adjacent to the side-by-side connectors. The data suggest a significant benefit in supplementing medial over lateral satellite rods at the PSO by reducing stress on the primary rods. Except the recessed short-rod technique, all other multirod constructs decrease the magnitude of the load acting across the osteotomy region, which could cause a delayed or non-union at the PSO site.

CLINICAL SIGNIFICANCE: The study evaluates the mechanical performance of various satellite rod instrumentation configurations following PSO to predict the risk factors for rod fracture and thereby mitigate the rate of clinically relevant failures.

Keywords: Biomechanics; Finite element analysis; Multirod constructs; Pedicle subtraction osteotomy; Rod fracture; Satellite rods; Spine.

Introduction

Sagittal imbalance can be associated with pain and mental and physical disabilities in patients with adult spinal deformity [1]. Among the restoration techniques, pedicle subtraction osteotomy (PSO) is a technique in which the posterior elements, pedicles, and a V-shaped section of the vertebral body are resected. Despite several advantages of the PSO in realigning spinal sagittal imbalance, it is a challenging procedure and associated with significant complications. The reported complication rates following PSO range from 37% to 59% [2,3]. One frequent delayed complication is rod fracture which has been reported to occur as often as 31.6% [4].

To decrease the rod fracture rate following PSO, various approaches such as the use of interbody spacers at the disc spaces adjacent to the PSO, utilizing one or more satellite rods, and choosing stiffer cobalt chromium (CoCr) rods have been shown to be clinically beneficial [4–8]. Despite several efforts to study the effects of the PSO in recent years, there are few computational studies investigating mechanical parameters [9–12]. In those simulations, either a simplified model was used or only a few instrumentation configurations were considered. The overall objective of the current study was to perform a finite element analysis (FEA) to evaluate the mechanical aspects of various multirod instrumentation constructs for the PSO procedure.

Material and methods

In this study, a previously validated osseoligamentous three-dimensional (3-D) spinopelvic model (T10-pelvis) [13–15] was used to develop a PSO at the L3 level. The geometry of the intact model of the ligamentous spine was reconstructed in MIMICS (Materialize Inc., Leuven, Belgium) software from computed tomography (CT) scans of a human spine. The hexahedral elements (C3D8) on the vertebrae and tetrahedral elements (C3D4) on the pelvis were created using IAFE-MESH (University of Iowa, Iowa) and HyperMesh (Altair Engineering, Michigan, USA) software. Subsequently, all the meshed components were assembled in the Abaqus 6.14 (Dassault Systèmes, Simulia Inc., Providence, RI, USA) software for analysis. The trabecular bones of the vertebrae and pelvis were surrounded by 0.5 mm and 1 mm layer of cortical bone in the model, respectively [16–20]. The ligamentous tissues including spinal and sacroiliac joint

Table 1
Material properties of the models' components [16–18]

Component	Element formulation	Modulus (MPa)/poisson's ratio
Vertebral cortical bone	Isotropic, elastic hex elements (C3D8)	12000/0.3
Vertebral cancellous bone	Isotropic, elastic hex elements (C3D8)	100/0.2
Pelvic cortical bone	Isotropic, elastic hex elements (C3D8)	17000/0.3
Pelvic cancellous bone	Isotropic, elastic hex elements (C3D8)	10/0.2
Annulus (ground)	Neo-Hookean, hex elements (C3D8)	C10 = 0.348, D1 = 0.3
Annulus (fiber)	Rebar	357–550
Nucleus	Mooney Rivlin hex elements (C3D8H)	C1 = 0.12, C2 = 0.03, D1 = 0.0005
Apophyseal joints	Nonlinear soft contact, GAPUNI elements	–
Sacroiliac joints	Nonlinear soft contact	–
Ligaments	Hypo-elastic, tension only, Truss elements (T3D2)	Nonlinear stress–strain curves
Ti6Al4V pedicle screws	Isotropic, tetrahedron elements (C3D4)	11500/0.3
CoCr rods	Isotropic, tetrahedron elements (C3D4)	241000/0.3

ligaments were simulated using truss elements. The material properties of the model components were extracted from previous studies (Table 1) [17,21,22].

The T10-pelvis intact spinal model was modified to simulate a PSO at the L3 level. To achieve this, posterior elements including posterior arch, posterior longitudinal ligaments, transverse ligaments, interspinous ligaments, and supraspinous ligaments were removed initially. Subsequently, along with pedicles and facet joint removal, a wedge-shaped bone resection of 30° was performed at the vertebral body of the L3. The spinopelvic PSO model was composed of 154,475 elements and 110,061 nodes. A surface to surface contact with a friction of 0.46 was defined between the two resected extremities [23].

The instrumentation including pedicle screws, rods, and side-by-side connectors were designed in SolidWorks (Dassault Systèmes SolidWorks Corporation, Waltham, MA, USA) software and imported into Abaqus for meshing and analysis. The pedicles of T10, T11, and T12 vertebral levels were instrumented bilaterally with titanium alloy (Ti6Al4V) 4.5 mm pedicle screws with the length of 40 mm. Six 5.5-mm pedicle screws with the length of 45 mm were anchored bilaterally in the L1, L2, and L4 pedicles. The L5 and S1 pedicles were instrumented with 6.5 mm screws with the length of 45 mm and 55 mm, respectively. Two 8.5-mm iliac screws with the length of 80 mm were placed such that there was no screw prominence. 5.5 mm primary rods were connected bilaterally to the pedicle screw tulips extending from T10 to the iliac screws. The pedicle screw sizes were chosen based on model pedicle dimensions and were consistent among various instrumentation configurations.

Overall, the following five instrumentation configurations were analyzed (Fig. 1).

- PSO instrumented with bilateral primary rods from T10 to pelvis. (PSO+primary rods [PR]).
- PSO instrumented with bilateral primary rods from T10 to pelvis and medially affixed satellite rods connected to the primary rods above the L2 and below the L4 pedicle screws. (PSO+medial satellite rods [MSR]).
- PSO instrumented with bilateral primary rods from T10 to pelvis and laterally affixed satellite rods connected to the primary rods below the L1 and above the L5 pedicle screws. (PSO+lateral satellite rods [LSR]).
- PSO instrumented with bilateral primary rods from T10 to pelvis and posteriorly affixed satellite rods connected to the L1 and L5 pedicle screw levels. Pedicle screws used in these levels were a novel design called "head-to-head" technique patented by Frankel et al. In this technique, the screw system comprises two different tulip heads to connect multiple rods [24]. (PSO+posterior satellite rods [PSR]).
- PSO instrumented with a novel multirod technique (short-rod technique) proposed by Gupta et al. [25]. In this technique, the primary rods were not attached to the pedicle screws anchored adjacent to the PSO level, while two recessed supplementary short rods were spanning only the PSO level using anchors connected to the adjacent levels (SRT).

Loading and boundary conditions

The loading for the PSO spinopelvic FEA models was applied in two different steps. In the first step, as previously published by Patwardhan et al. [26], 300 N to the thoracic spine and 400 N to the lumbar spine were applied using follower load technique. In the second step, pure moments of 7.5 Nm were applied to the top endplate of the T10 vertebral body in all three anatomical directions. During the simulation steps, the acetabulum surfaces of the pelvis were fixed in all degrees of freedom.

Finite element model validation

The developed human T10-pelvis model was previously validated under static and dynamic loading. For this purpose, the segmental kinematic data across the spine were compared to those obtained from a cadaveric experiment and literature in flexion, extension, lateral bending, and axial rotation motions [15]. Final data analysis for this study utilized CoCr rods. However, to validate our FE model, we performed additional simulations (PSO+PR and PSO+MSR) by changing the rods material properties to titanium and compared to the accepted experimental study by Hallager et al., in which the titanium rods were utilized [27]. In this regard, in different directions, L2–L4 range of motions (ROM) of the instrumented PSO+PR (bilateral primary rods) and PSO+MSR models were normalized to the intact condition (no PSO and instrumentation) and compared to the cadaveric study conducted by Hallager et al. Additionally, the average strain on both primary and satellite rods for the PSO+PR and PSO+MSR constructs were normalized to the PSO construct instrumented with bilateral titanium primary rods and compared to the Hallager et al. experimental study [27].

To validate the numerical accuracy of the simulations, a mesh convergence study was additionally performed on the instrumented models. The model was considered to be converged if by increasing the number of elements the maximum von Mises stress on the rods varied less than 4%.

Data analysis

L2–L4 ROM and average strain at the PSO level of the rods in instrumented PSO+PR and PSO+MSR models were analyzed for validation purposes. T10-S1 global ROM of all the instrumented models in all directions was calculated. For all the constructs, the stress distribution plots on the rods were evaluated. In addition, the values for the maximum von Mises stress on the rods and at the PSO level and force at the PSO resected region were recorded and compared for all the models. Stress values within important regions were used to calculate the factor of safety (FOS) of different constructs [28]. For this analysis, FOS was defined as the ratio of the CoCr yield stress (928 MPa) to maximum recorded von Mises stress in the rod for a given loading condition. The higher the FOS the lesser the chances of rod fracture. To compare the force values acting at the osteotomy site among various constructs, the values were obtained following follower load application. Fig. 2 highlights the location where the force values were collected.

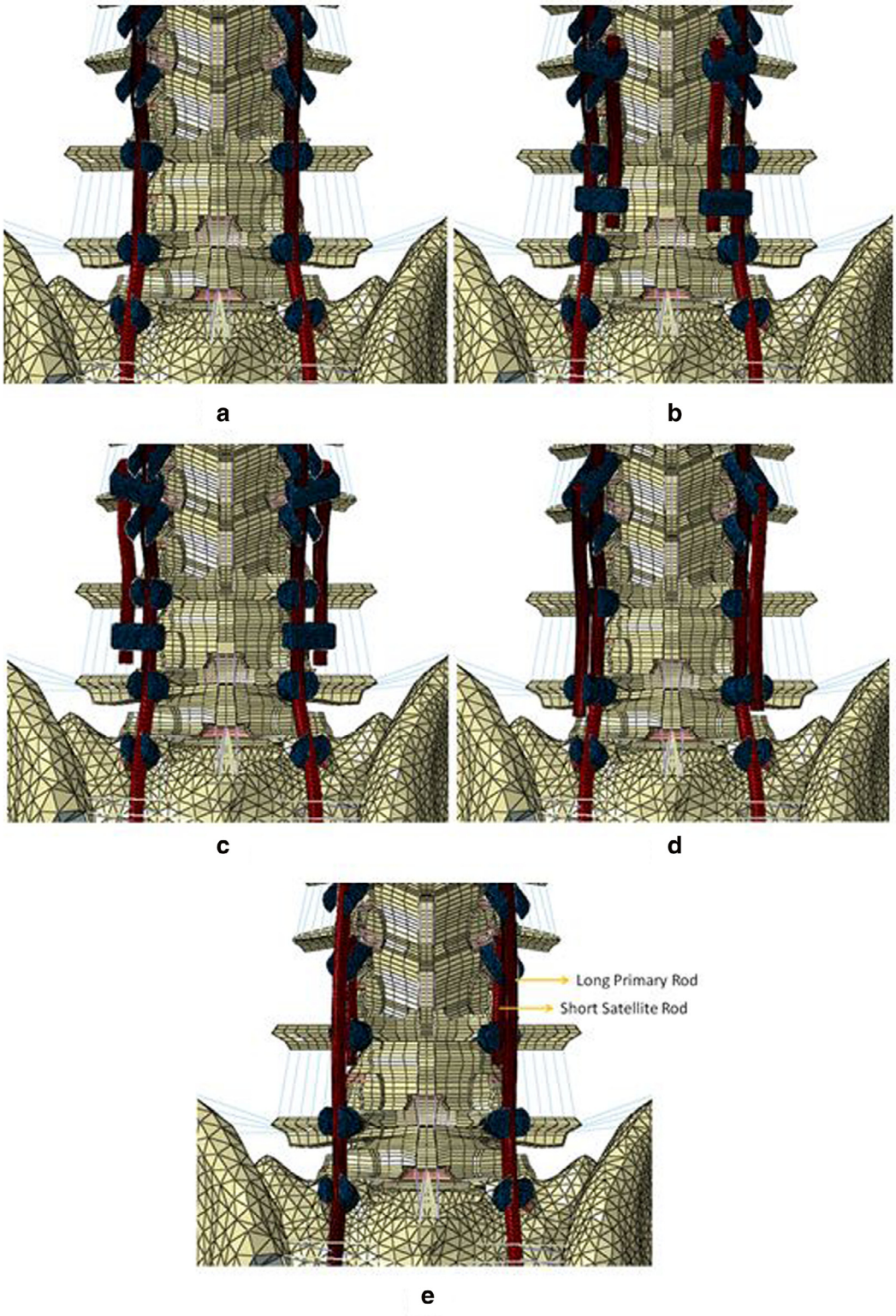

Fig. 1. Posterior view of various instrumentation configurations following PSO. (a) Bilaterally instrumented PSO model (PSO+PR). (b) Four-rod instrumented PSO supplemented with medially affixed satellite rods (PSO+MSR). (c) Four-rod instrumented PSO supplemented with laterally affixed satellite rods (PSO+LSR). (d) Four-rod instrumented PSO supplemented with posteriorly affixed satellite rods (PSO+PSR). (e) Four-rod instrumented PSO with short-rod technique (SRT). PSO, pedicle subtraction osteotomy.

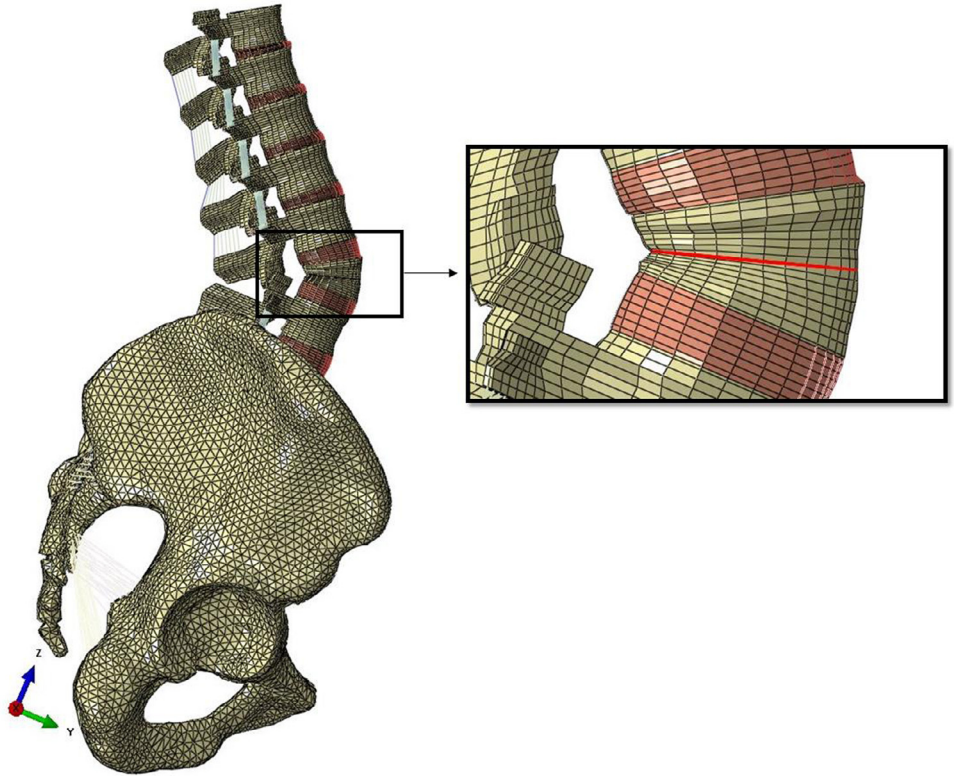

Fig. 2. Lateral view of pedicle subtraction osteotomy finite element model. The magnified image highlights the PSO surface where forces were collected. PSO, pedicle subtraction osteotomy.

Results

Model validation

The validation graph for the L2–L4 ROMs of the instrumented PSO+PR (bilateral primary rods) and PSO+MSR models normalized to the intact condition (no PSO and instrumentation) is illustrated in Fig. 3. The data was compared to in vitro study conducted by Hallager et al. [27]. FEA predictions for all the loading directions were close to average in flexion-extension and lateral bending and within one standard deviation in axial rotation cases.

Fig. 4 shows the average strain on both primary and satellite rods (in the case of four-rod construct) during flexion-extension in PSO+PR and PSO+MSR models normalized to the titanium bilateral primary rods. Strain results on the rods for both constructs were in a good agreement with the cadaveric study of Hallager et al. [27]. Thus, our spinopelvic PSO instrumented models behave similarly to the in vitro studies under various loading directions.

ROM

Overall, a reduction of T10-S1 global ROM was recorded when satellite rods were added to the PSO instrumented spinopelvic model. Compared to the PSO+PR construct, PSO +MSR configuration showed approximately 15%, 16%, 3%, and 8% reduction in flexion, extension, lateral bending, and axial rotation motions, respectively. In the PSO+LSR model, a similar trend of motion reduction was observed. In this model, the motion reduction, as compared to the PSO+PR model, ranged between 1% and 12%, recorded during the lateral bending and extension, respectively. Among all multirod constructs, PSO+PSR showed the greatest motion reduction as compared to the instrumented PSO+PR configuration. Compared to the PSO+PR model, the PSO+PSR construct reduced flexion and extension by 36%, lateral bending by 17%, and axial rotation by 10%. The use of short-rod technique (SRT) resulted in 11%, 4%, and 49% reduction in T10-S1 flexion, extension, and lateral bending motions compared to the PSO+PR, respectively, while the axial rotation motion increased by about 31%. A comparison of the instrumented T10-S1 global ROM in different loading directions and configurations is shown in Fig. 5.

Von Mises stress results on the rods

Maximum von Mises stress on the rods

In all the constructs with the exception of SRT, the maximum von Mises stress on the rods occurred with flexion. In the PSO+PR construct, the greatest von Mises stress recorded on the rods was at or adjacent to the PSO level where the rods were highly contoured. In contrast to the PSO +PR construct, in PSO+MSR configuration, the location of the maximum von Mises stress was on the primary rods and shifting adjacent to the side-by-side connectors. Similar to the PSO+MSR construct, in the PSO+LSR configuration, the

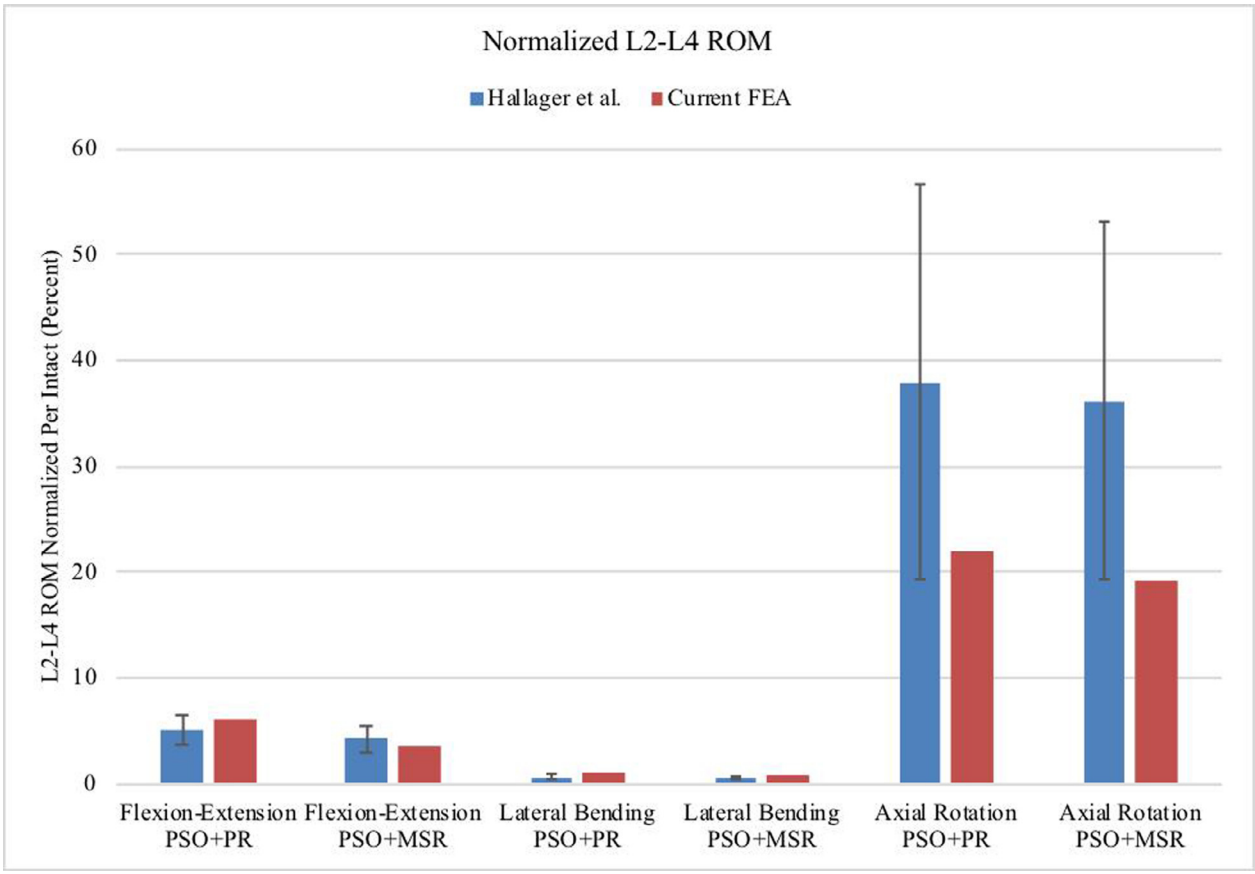

Fig. 3. The L2–L4 range of motion validation results for the PSO+PR (bilateral primary rods) and PSO+MSR (medially satellite rods) constructs in different loading directions (flexion-extension, lateral bending, and axial rotation). PSO, pedicle subtraction osteotomy.

location of the maximum von Mises stress was on the primary rods and adjacent to the side-by-side connectors. Compared to the PSO+PR construct, PSO+PSR showed a significant reduction (9%–42%) in the maximum von Mises stress values in all the loading cases. In this construct, the maximum von Mises stress occurred on the primary rods and adjacent to the anchors where the satellite rods were connected. The greatest reduction in the maximum von Mises stress on the rods was recorded in the SRT configuration. In this technique, the maximum von Mises stress occurred on

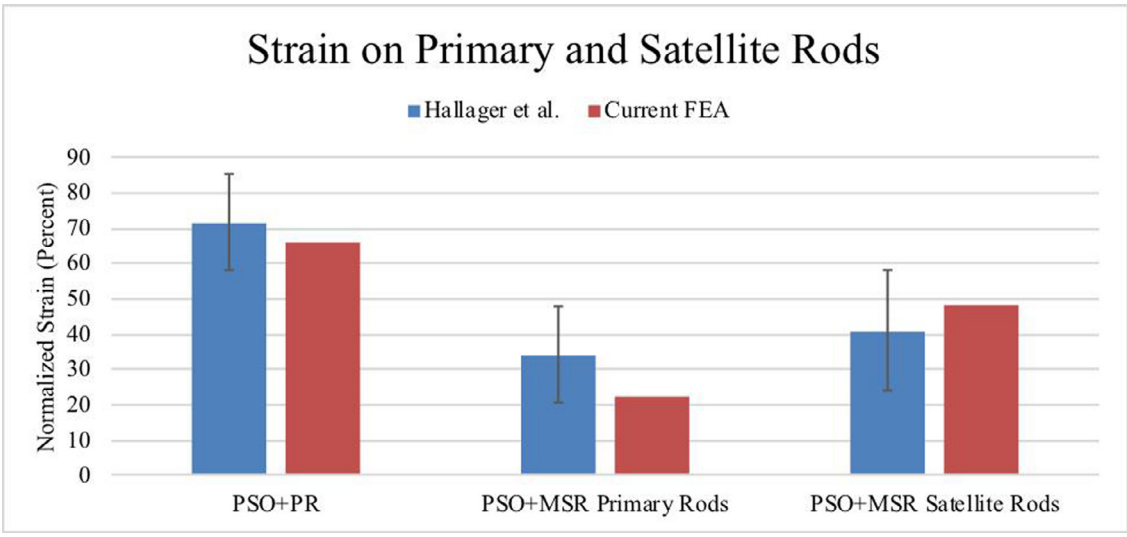

Fig. 4. Average strains on both primary and satellite rods during flexion-extension, normalized to titanium bilateral primary rods.

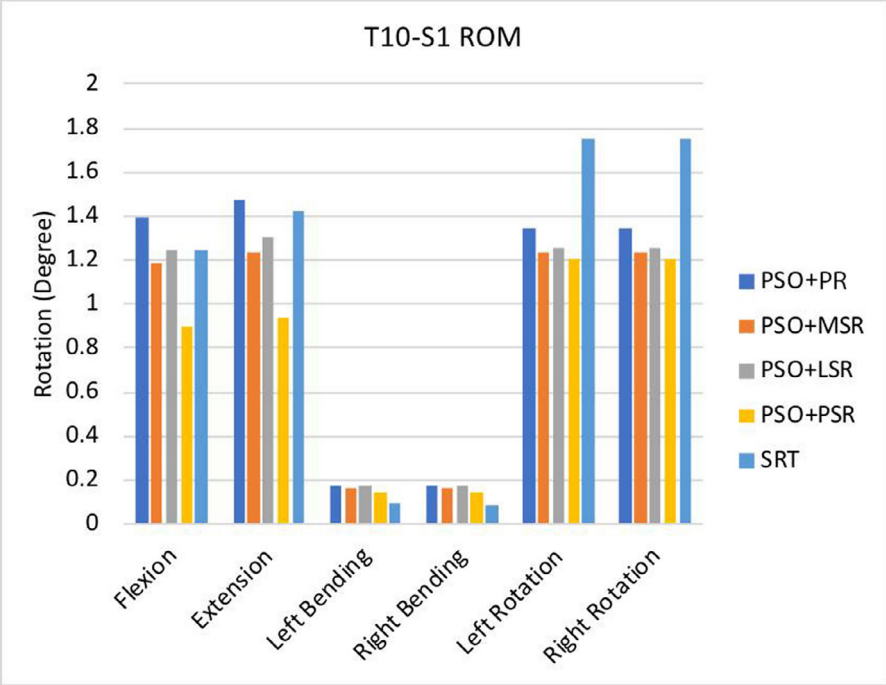

Fig. 5. Comparison of the instrumented T10-S1 global ROM for different loading directions and configurations.

the long primary rods. Table 3 shows the values and locations of maximum von Mises stress recorded on the rods for various configurations and motions with respect to the PSO +PR construct. This table also includes the FOS of the constructs. Among all multirod constructs, the SRT showed the greatest FOS value followed by PSO+PSR, then PSO+MSR and finally PSO+LSR.

Maximum von Mises stress at the PSO level (L3 level) on the rods

The addition of satellite rods considerably reduced the maximum von Mises stress values on the primary rods at the PSO level. In the medially affixed multi-rod construct (PSO+MSR), during various motions, the maximum von Mises stress recorded at the PSO level was greater in the

Table 2
Values and locations of the maximum von Mises stress (MPa) and corresponding factor of safety recorded on the rods for various configurations in different motions with respect to the PSO+PR construct. Actual stress values and locations shown for the PSO+PR construct, locations and percent difference from PSO+PR shown for others

Test condition	PSO+PR	PSO+MSR	PSO+LSR	PSO+PSR	SRT
Flexion	339 PSO	−8% Adjacent to connector (primary rod)	−4% Adjacent to connector (primary rod)	−30% L5−S1	−34% L5−S1 (primary rods)
Extension	105 L4−L5	−2% Adjacent to connector (primary rod)	+5% Adjacent to connector (primary rod)	−9% L5−S1	−10% L5−S1 (primary rods)
Left bending	221 PSO (right rod)	−3% Adjacent to connector (primary rod)	0% Adjacent to connector (primary rod)	−30% L5−S1(right primary rod)	−12% L5−S1 (Primary rods)
Right bending	221 PSO (left rod)	−3% Adjacent to connector (primary rod)	+3% Adjacent to connector (primary rod)	−32% L5−S1(left primary rod)	−14% L5−S1 (Primary rods)
Left rotation	256 PSO (right rod)	+2% Adjacent to connector (primary rod)	+11% Adjacent to connector (primary rod)	−40% T12−L1 & L5−S1 (right primary rod)	−11% L1−L5 (Primary rods)
Right rotation	256 PSO (left rod)	0% Adjacent to connector (primary rod)	+8% Adjacent to connector (primary rod)	−42% T12−L1 & L5−S1 (left primary rod)	−12% L1−L5 (primary rods)
Factor of safety	2.7	3	2.8	3.9	4.1

Table 3
The Values and locations of the maximum von Mises stress (MPa) and corresponding factor of safety recorded on the rods at the PSO level for various configurations in different motions with respect to the PSO+PR construct. Actual stress values and locations shown for the PSO+PR construct, locations and percent difference from PSO+PR shown for others

Test condition	PSO+PR	PSO+MSR	PSO+LSR	PSO+PSR	SRT
Flexion	339 Both rods	−34% Both satellite rods	−22% Both primary rods	−42% Both satellite rods	−48% All rods
Extension	73 Both rods	−40% Both satellite rods	−38% Both primary rods	+1% Both primary rods	−1% Shorter rods
Left bending	221 Left rod	−27% Right satellite rod	−19% Right primary rod	−30% Right satellite rod	−42% All rods except left long rod
Right bending	221 Right rod	−24% Left satellite rod	−21% Left primary rod	−32% Left satellite rod	−40% All rods except right long rod
Left rotation	256 Right rod	−40% Right satellite rod	−24% Right primary rod	−40% Right satellite rod	−11% Longer rods
Right rotation	256 Left rod	−41% Left satellite rod	−26% Left primary rod	−42% Left satellite rod	−12% Longer rods
Factor of safety	2.7	4.1	3.5	4.7	4.1

Table 4
Magnitudes of the load acting on the PSO region after follower load application in various instrumentation configurations

Instrumentation configuration	Force magnitude (N)
PSO+PR	248
PSO+MSR	208.9
PSO+LSR	221.9
PSO+PSR	156.5
SRT	247.6

satellite rods than in the primary rods. However, in the laterally affixed multirod construct (PSO+LSR) this value at the PSO level was greater on the primary rods, as compared to the laterally placed satellite rods. In general, the maximum von Mises stress values recorded at the PSO level on the rods for PSO+LSR were greater than the PSO+MSR and lower than the PSO+PR configuration. During all the loading directions, except extension, the maximum von Mises stress at the PSO level in the PSO+PSR construct occurred on the satellite rods. Compared to the PSO+PR construct, the SRT configuration reduced the maximum von Mises stress values from 1% to 48% in various motions, at the PSO level. Table 2 shows the values and locations of maximum von Mises stress recorded on the rods at the PSO level for various configurations and motions with respect to the PSO+PR construct. This table also includes the FOS of the constructs at the PSO level. Among all multirod constructs, at the PSO level, the PSO +PSR showed the greatest FOS value followed by SRT and PSO+MSR, followed by PSO+LSR.

Force at the osteotomy region

Compared to the PSO+PR construct, the load magnitude acting on the osteotomy site decreased by 16%, 11%, and 37% in the PSO+MSR, PSO+LSR, and PSO+PSR constructs, respectively (Table 4). SRT configuration showed similar force value to the PSO+PR construct.

Discussion

The results of our FEA indicated that the addition of satellite rods to the two-rod instrumented PSO+PR construct decreased the T10-S1 global ROM in all directions. In addition, FEA outcomes showed that the use of CoCr rods over titanium rods during flexion-extension in PSO+PR construct reduced the average strain values at the PSO level of the rods. The results also highlighted that in the PSO+MSR construct although both primary and satellite rods indicated reduced average strain values with the addition of satellite rods, strain further migrated to the satellite rods. Hallager et al. in an in vitro study evaluated the effect of adding two short precontoured medially SR on the ROM and rods' strain after PSO. The authors observed that the satellite and CoCr rods provide the greatest reduction in motion and strain at the PSO level [27]. Our observations are in a good agreement with these prior in vitro findings [27].

Hyun et al. compared the rod fracture rate in standard two-rod constructs to multirod constructs following three-column osteotomies [8]. Their retrospective study exhibited a significantly greater complete instrument failure at the PSO site in two-rod constructs than the multirod constructs (11 failures vs. 0 failures). The results of our computational study also indicated that by adding satellite rods the maximum von Mises stress magnitudes on the rods at the PSO level reduced up to 42%. In general, having multiple rods connected together using side-by-side connectors modifies the moment of inertia leading to different stress distributions on the instrumentations [10]. Lower stress values at the PSO level of the rods results in a lower risk of rod failure at this site. The addition of any satellite rod would lead to an increase in metal bulk, which could result in additional metal artifact with postoperative imaging. Additionally, some satellite constructs could interfere with the

fusion mass and a tension-free wound closure. Lateral and PSR could affect wound closure and the LSR could limit the posterior lateral fusion mass, as compared to recessed short-rods and MSR. In several multirod cases, by adding satellite rods the location of maximum von Mises stress on the rods in different motions occurred adjacent to the side-by-side connectors. These findings give possible explanation to the previously reported high rate of rod failure adjacent to the satellite rods [29]. The stress concentration at these areas can be due to the transition from more rigid two-bonded rods segment (primary and satellite rods) to the less rigid single (primary rod) segment. The FOS results also signified that among all multirod constructs, SRT (FOS = 4.1) has the greatest load bearing capacity followed by
PSO+PSR (FOS = 3.9), then PSO+MSR (FOS = 3) and finally PSO+LSR (FOS = 2.8). However, considering the maximum von Mises stress at the PSO level of the rods, the PSO+PSR is the safest construct with the greatest FOS (FOS = 4.7) followed by SRT and PSO+MSR (FOS = 4.1) and finally PSO+LSR (FOS = 3.5).

In the biomechanical study of Hallager et al., the authors reported that with the medially placed satellite rods in the four-rod constructs greater strain recorded was on the accessory rods [27]. Additionally, Luca et al. conducted a finite element study on the similar constructs with titanium alloy rods and recorded greater maximum von Mises stress at the PSO region of medially placed satellite rods [10]. The current FEA indicated that in the PSO+MSR and PSO +LSR constructs, the maximum von Mises stress at the PSO level occurred on the medial rods. At the PSO level, in the PSO+MSR construct the greater maximum von Mises stress was recorded on the satellite rods, while in the PSO+LSR construct it was on the primary rods. These observations show that at the PSO level in the PSO+MSR construct there is a greater risk of rod fracture in satellite rods, while in the PSO+LSR it is in primary rods. Additionally, the maximum von Mises stress magnitudes recorded at the PSO region was greater in the PSO+LSR configuration, compared to the PSO+MSR configuration implying a higher risk of rod failure in the PSO+LSR construct. These findings exhibit a significant advantage in supplementing medially placed satellite rods over the laterally affixed satellite rods, as there is less stress observed in the PSO+MSR construct, and even in the event of rod fracture at the PSO level, the surgeon can more easily replace shorter satellite rods, as compared to longer primary rods secured to multiple pedicle screw tulips.

The novel pedicle screw design patented by Frankel et al. allows for the posterior connection between the satellite rods and the primary rods [24]. Albeit these screws have not been manufactured or tested before, the results of our FEA were promising. In the PSO+PSR configuration, the location of maximum von Mises stress in different loading scenarios occurred either adjacent to the anchors where the satellite rods ended or at the PSO level. Similar to the PSO+MSR and PSO+LSR constructs, due to transition in the rigidity from two-rod to one-rod section, the stress concentration adjacent to these anchors was high. In flexion motion, PSO+PSR construct reduces the maximum von Mises stress on the rods more than the PSO+MSR and PSO+LSR configurations. Similarly, Luca et al. in a finite element study of instrumentation failure following PSO noted that placing the satellite rods posteriorly allowed for more stress reduction on the instrumentation [10]. In current study, due to difference in fixation techniques, in the PSO+PSR construct the satellite rods span from the L1 to L5 pedicle screw tulips, while in PSO+MSR and PSO+LSR the satellite rods are connected through side-by-side connectors below the L1 and above the L5 pedicle screws, respectively. Despite the similarities in these constructs, the minor difference in spanning region for the satellite rods could affect the rigidity of the constructs and alter mechanical parameters.

Gupta et al. have recently reported on the SRT in which the primary rods were not attached to the pedicle screws anchored adjacent to the PSO level, while two recessed supplementary short rods were spanning only the PSO level using anchors connected to the adjacent levels [25]. They compared the rod fracture rate using this novel method with the traditional two-rod technique, and recorded 0 % rod failure with four rods, compared to 25% fracture rate with two rods. For this construct, our FEA also shows a significant reduction in the maximum von Mises stress values in different directions compared to the two-rod construct. With SRT, the longer primary rods are not connected to the pedicle screws and rods immediately adjacent to the PSO, averting a need for acute rod contouring at this region. In this regard, Tang et al. conducted a biomechanical study on the severity of rod contour in a PSO setting and found that more severe angles of rod contour have a greater risk of failure, and the fatigue life of the rods depends significantly on the severity of the rod contour [30].

Similar to Luca et al. observations that adding two accessory rods medially enhances the posterior force on the instrumentation, our results showed that subsequent to follower load application in all multirod constructs the load acting on the PSO region decreased [10]. Adding accessory rods increases the stiffness of the instrumentation, which results in a greater load transfer to the posterior instrumentation, leading to a reduction in the load acting across the osteotomy site. Among all multirod constructs, the closest force magnitude recorded at the osteotomy region to the PSO+PR configuration was seen in the SRT construct.

Bone healing is a complex process which is affected by various factors. The dynamics and distribution of the mechanical loading, bone cells and mechanical receptors, blood perfusion, metabolite supplementation, growth factors, cytokines, and hormones are among the significant factors influencing bone fracture healing [31–35]. According to the Wolff's Laws, the mechanical forces influence bone formation and remodeling [36]. In bone fracture

healing, excessive strain on the fracture site results in instability followed by delayed healing or nonunion. Conversely, too rigid instrumentation can often cause limited strain at the fracture site, which may be inadequate to stimulate the bone formation. As a result of the inadequate stimulus, callus formation may be insufficient, resulting in nonunion [37,38]. Our findings showed that with the use of multirod constructs (except SRT) the magnitude of the force acting across the osteotomy site decreased significantly. Even though multirod constructs decrease the rod fracture rate by reducing the maximum von Mises stress, due to force reduction on the anterior column this may delay or inhibit bony union across the PSO site. In this regard, the SRT not only provided similar forces across the anterior column, but it was also accompanied with a significant maximum von Mises stress reduction on the rods.

This is the first study which has investigated the global ROM, instrumentation stress, and load application on the osteotomy region for various PSO multirod instrumentation techniques extending from the thoracic spine to the pelvis. The data can be used to address various biomechanical questions regarding different instrumentation techniques when performing a PSO. For example, the failure location of the bilateral primary rods PSO instrumentation is expected to be at or adjacent to the PSO level, while in most of the four-rod configurations it shifts to the more rigid location where multiple rods are attached via side-by-side connectors. Therefore, the findings of this study would be useful to understand and compare the biomechanical differences between various multirod instrumentation of the PSO construct.

Similar to any other FEA, the limitations of the current computational study should also be taken into account. Unavailability of the ROM data for the osteoligamentous spine associated with PSO is a limitation of this study. A second important limitation of the current study was that no muscle forces were simulated in the models. However, this limitation was mitigated using the follower load method as previously published by Patwardhan et al. [26]. Additionally, contacts, constraints, and the geometries of the implants in the models were simplified, and the index surgery procedure was not simulated. In this regard, the simulation of the residual stress on the rods and other components, which is caused by intraoperative contouring and the spine instrumentation maneuvers, was neglected in the models. Dynamic analysis of the components such as fatigue test provides more accurate failure assessment of the rods. No dynamic analysis was simulated in this study, and fatigue testing of different constructs of the current FE study is suggested for future assessments.

Conclusions

In multirod constructs, adding multiple satellite rods increases the stability of the construct. Among all multirod constructs, the greatest motion reduction in all directions was observed with the use of posteriorly affixed four-rod technique, followed by medially and laterally affixed satellite rods. At the PSO level, these constructs decrease the maximum von Mises stress on the rods. The von Mises stress values showed that the SRT has the lowest risk of rod failure (greatest FOS defined as yield stress of the rod material/maximum actual stress in the rod), followed by the PSO+PSR, PSO+MSR, and PSO+LSR constructs. Comparing the maximum stress values at the PSO level on the rods, there is a benefit in supplementing medially affixed satellite rods over the laterally affixed satellite rods to augment the PSO, which also does not prohibit bone grafting in the lateral gutters or wound closure. The assessment of the load acting on the osteotomy region also signified that except SRT, all other multirod constructs decrease the magnitude of the load acting across the osteotomy site, which may cause a delayed union or nonunion of the PSO site. In conclusion, the study evaluated the mechanical performance of various satellite rod instrumentation configurations following PSO to predict the risk factors for rod fracture and thereby mitigate the rate of clinically relevant failures.

Acknowledgment

This study was supported partly by National Science Foundation (NSF) IIP-136197 Industry/University Cooperative Research Center at the University of California, San Francisco, CA and The University of Toledo, Toledo, OH (www.nsfcdmi.org).

References

[1] Yamato Y, Hasegawa T, Kobayashi S, Yasuda T, Togawa D, Arima H, et al. Calculation of the target lumbar lordosis angle for restoring an optimal pelvic tilt in elderly patients with adult spinal deformity. Spine 2016;41:E211–7.

[2] Smith JS, Sansur CA, Donaldson III WF, Perra JH, Mudiyam R, Choma TJ, et al. Short-term morbidity and mortality associated with correction of thoracolumbar fixed sagittal plane deformity: a report from the Scoliosis Research Society Morbidity and Mortality Committee. Spine 2011;36:958–64.

[3] Charles YP, Yu B, Steib J-P. Sacroiliac joint luxation after pedicle subtraction osteotomy: report of two cases and analysis of failure mechanism. Eur Spine J 2016;25:63–74.

[4] Smith JS, Shaffrey E, Klineberg E, Shaffrey CI, Lafage V, Schwab FJ, et al. Prospective multicenter assessment of risk factors for rod fracture following surgery for adult spinal deformity. J Neurosurg: Spine 2014;21:994–1003.

[5] Smith JS, Shaffrey CI, Ames CP, Demakakos J, Fu K-MG, Keshavarzi S, et al. Assessment of symptomatic rod fracture after posterior instrumented fusion for adult spinal deformity. Neurosurgery 2012;71:862–8.

[6] Barrey C, Perrin G, Michel F, Vital J-M, Obeid I. Pedicle subtraction osteotomy in the lumbar spine: indications, technical aspects, results and complications. Eur J Orthop Surg Traumatol 2014;24:21–30.

[7] Cho K-J, Kim K-T, Kim W-J, Lee S-H, Jung J-H, Kim Y-T, et al. Pedicle subtraction osteotomy in elderly patients with degenerative sagittal imbalance. Spine 2013;38:E1561–6.

[8] Hyun S-J, Lenke LG, Kim Y-C, Koester LA, Blanke KM. Comparison of standard 2-rod constructs to multiple-rod constructs for fixation across 3-column spinal osteotomies. Spine 2014;39:1899–904.

[9] Charosky S, Moreno P, Maxy P. Instability and instrumentation failures after a PSO: a finite element analysis. Eur Spine J 2014;23:2340–9.
[10] Luca A, Ottardi C, Sasso M, Prosdocimo L, Barbera LL, Brayda-Bruno M, et al. Instrumentation failure following pedicle subtraction osteotomy: the role of rod material, diameter, and multi-rod constructs. Eur Spine J 2017;26:764–70.
[11] Luca A, Ottardi C, Lovi A, Brayda-Bruno M, Villa T, Galbusera F. Anterior support reduces the stresses on the posterior instrumentation after pedicle subtraction osteotomy: a finite-element study. Eur Spine J 2017;26:450–6.
[12] Ottardi C, Galbusera F, Luca A, Prosdocimo L, Sasso M, Brayda-Bruno M, et al. Finite element analysis of the lumbar destabilization following pedicle subtraction osteotomy. Med Eng Phys 2016;38:506–9.
[13] Goel VK, Grauer JN, Patel TC, Biyani A, Sairyo K, Vishnubhotla S, et al. Effects of charite artificial disc on the implanted and adjacent spinal segments mechanics using a hybrid testing protocol. Spine 2005;30:2755–64.
[14] Goel VK, Mehta A, Jangra J, Faizan A, Kiapour A, Hoy RW, et al. Anatomic facet replacement system (AFRS) restoration of lumbar segment mechanics to intact: a finite element study and in vitro cadaver investigation. SAS J 2007;1:46–54.
[15] Palepu V. Biomechanical effects of initial occupant seated posture due to rear end impact injury. The University of Toledo; 2013.
[16] Edwards WT, Zheng Y, Ferrara LA, Yuan HA. Structural features and thickness of the vertebral cortex in the thoracolumbar spine. Spine 2001;26:218–25.
[17] Joukar A, Shah A, Kiapour A, Vosoughi AS, Duhon B, Agarwal AK, et al. Sex specific sacroiliac joint biomechanics during standing upright: a finite element study. Spine 2018;43:E1053–60.
[18] Bruna-Rosso C, Arnoux P-J, Bianco R-J, Godio-Raboutet Y, Fradet L, Aubin C-É. Finite element analysis of sacroiliac joint fixation under compression loads. Int J Spine Surg 2016;10:16.
[19] Kiapour A. Investigation into lumbar spine biomechanics of 360 motion preservation systems. 2010.
[20] Seyed Vosoughi A. Mitigating the biomechanical complications following pedicle subtraction osteotomy: a finite element analysis. 2017.
[21] Ivanov AA, Kiapour A, Ebraheim NA, Goel V. Lumbar fusion leads to increases in angular motion and stress across sacroiliac joint: a finite element study. Spine 2009;34:E162–9.
[22] Lindsey DP, Kiapour A, Yerby SA, Goel VK. Sacroiliac joint fusion minimally affects adjacent lumbar segment motion: a finite element study. Int J Spine Surg 2015;9.
[23] Goffin JM, Pankaj P, Hamish Simpson A. A computational study on the effect of fracture intrusion distance in three−and four−part trochanteric fractures treated with Gamma nail and sliding hip screw. J Orthop Res 2014;32:39–45.
[24] Frankel B, Semler ME, Walker C, and Fedorov S. Percutaneous modular head-to-head cross connector. U.S. Patent 9,023,087, issued May 5, 2015.
[25] Gupta S, Eski MS, Durbin-Johnson B, Ames C, Deviren V, Gupta M. Four rods prevent rod breakage and pseudarthrosis in pedicle subtraction osteotomies: GP243. Spine J Meet Abstr 2014: 269–70. LWW.
[26] Patwardhan AG, Havey RM, Carandang G, Simonds J, Voronov LI, Ghanayem AJ, et al. Effect of compressive follower preload on the flexion—extension response of the human lumbar spine. J Orthop Res 2003;21:540–6.
[27] Hallager DW, Gehrchen M, Dahl B, Harris JA, Gudipally M, Jenkins S, et al. Use of supplemental short pre-contoured accessory rods and cobalt chrome alloy posterior rods reduces primary rod strain and range of motion across the pedicle subtraction osteotomy level: an in vitro biomechanical study. Spine 2016;41:E388–95.
[28] Hill G, Nagaraja S, Bridges A, Vosoughi AS, Goel VK, Dreher ML. Mechanical performance of traditional distraction-based dual growing rod constructs. Spine J 2018. https://doi.org/10.1016/j.spinee.2018.09.006.
[29] Shen FH, Qureshi R, Tyger R, Lehman R, Singla A, Shimer A, et al. Use of the “dual construct” for the management of complex spinal reconstructions. Spine J 2018;18:482–90.
[30] Tang JA, Leasure JM, Smith JS, Buckley JM, Kondrashov D, Ames CP. Effect of severity of rod contour on posterior rod failure in the setting of lumbar pedicle subtraction osteotomy (PSO) a biomechanical study. Neurosurgery 2012;72:276–83.
[31] Burr DB, Robling AG, Turner CH. Effects of biomechanical stress on bones in animals. Bone 2002;30:781–6.
[32] Gardner TN, Evans M, Hardy J, Kenwright J. Dynamic interfragmentary motion in fractures during routine patient activity. Clin Orthop Relat Res 1997;336:216–25.
[33] Jagodzinski M, Krettek C. Effect of mechanical stability on fracture healing—an update. Injury 2007;38:S3–S10.
[34] Khan SN, Bostrom MP, Lane JM. Bone growth factors. Orthop Clin 2000;31:375–87.
[35] Skerry TM, Lanyon LE, Bitensky L, Chayen J. Early strain−related changes in enzyme activity in osteocytes following bone loading in vivo. J Bone Miner Res 1989;4:783–8.
[36] Wolff J. Du Gesetz der Transformation der Knochen. Stuttgart: Schattauer, Berlin: Hirschwald; 1892.
[37] Figueiredo U, Watkins P, Goodship A. The effects of micromotion in distraction osteogenesis. Trans Orthop Res Soc 1993;39:130.
[38] Klein-Nulend J, Van der Plas A, Semeins CM, Ajubi NE, Frangos JA, Nijweide PJ, et al. Sensitivity of osteocytes to biomechanical stress in vitro. FASEB J 1995;9:441–5.